ARTICLE

Journal of Materials Chemistry
www.rsc.org/materials

Study of the crystallinity of ZnO in the Zn/ZnO nanocable heterostructures†

Yuk-hong Wong and Quan Li*

Department of Physics, The Chinese University of Hong Kong, Shatin, New Territory, Hong Kong. E-mail: liquan@phy.cuhk.edu.hk; Fax: 2603 5204

Received 14th January 2004, Accepted 9th March 2004
First published as an Advance Article on the web 31st March 2004

Coaxial Zn/ZnO core–shell nanocable heterostructures with diameters ~100 nm were synthesized *via* thermal reduction of ZnO by H_2. The products were characterized by X-ray powder diffraction, scanning electron microscopy, transmission electron microscopy and cathodoluminescence. In some of the samples, an epitaxial relationship was found between the Zn core and the ZnO outer shell aside from the large lattice mismatch (17%) between Zn and ZnO. Systematic studies were carried out using different fabrication parameters in order to find out the formation mechanism of the ZnO layer with different crystallinity and the origin of the epitaxy between Zn and ZnO.

I. Introduction

Recently there has been great interest in one-dimensional (1D) nanometer-sized materials, such as nanotubes,[1,2] nanowires[3,4] and nanocables.[5–11] These 1D nanostructures may serve as both functional components and interconnects simultaneously in nanoscale electronics and optoelectronics[12–16] due to their specific dimensionality and various size-related novel properties. Much work has been devoted to the size,[2,17–20] morphology control[21–23] and the yield improvement[24,25] of the products. Among all these 1D nanostructures, nanocable is one of the most interesting types. The presence of interface(s) between different phases in the cable's radial direction, together with possible quantum confinement effects induced by the small size, may result in interesting properties. Inspired by this, many researchers have been focusing on the synthesis of various nanocables. By mechanism, nanocables may be formed by sequential deposition of the core and shell(s) materials (with core as the template for the shell(s)) as well as co-deposition of the core and shell(s) materials (with a spontaneous phase separation between the core and shell(s)). In the former case, Lieber and co-workers have reported Ge–Si, Si–Ge as well as multishell nanocables synthesized using chemical vapor deposition.[5] Yang and co-workers have synthesized Ge–C core–shell nanocables by thermal evaporation followed by annealing in organic vapor.[6] Xie and co-workers also fabricated CdS/CdSe nanocables by mixing CdS nanowires with Se powder followed by a heat treatment.[7] In the latter case, representative examples include Si/SiO_x core–shell nanocables formed by laser ablation of a $Si_{1-x}Fe_x$ target,[8] a three-layer-coaxial nanocable comprised of a silicon carbide core, an amorphous silicon oxide intermediate layer and an outer shell of carbon and boron nitride using reactive laser ablation,[9] CdSe/poly(vinyl acetate) nanocables synthesized by mixing the monomer solution and metal compound solution under γ-irradiation,[10] and Si/CdSe nanocables by one-step thermal evaporation of a CdSe powder on a pre-treated Si substrate.[11]

In this study, we are interested in Zn/ZnO nanocables. It is known that ZnO is one of the most promising semiconducting materials with extremely attractive optical, electrical, and piezoelectrical properties. In fact, several groups have been able to synthesize Zn/ZnO heterostructures using various physical/chemical methods.[26–29] The Zn/ZnO interface presented in the nanocable heterostructures acts as natural metal/semiconductor junction. Together with the special dimensionality, these make the Zn/ZnO nanocable an ideal candidate for functional building blocks in nanoelectronics/optoelectronics. The quality of the ZnO shell as well as the interface between Zn/ZnO are therefore of current interest, as they eventually determine the electrical/optical responses of the nanocables. In the present work, coaxial Zn/ZnO nanocables are synthesized using a vapor-phase transport process. An epitaxial relationship was found between the Zn core and the ZnO outer shell in some of the samples, despite a large lattice mismatch (17%) existing between Zn and ZnO. The crystallinity of the ZnO shell and its defect density (in nanocables synthesized under different experimental conditions) were systematically investigated in order to find out the formation mechanism of the ZnO layers with different crystallinity, and the origin of the epitaxy between Zn and ZnO. The driving force for the formation of such a coaxial structure is discussed.

II. Experimental

The Zn/ZnO nanocables were fabricated by thermal reduction reaction between ZnO and H_2. The reaction took place inside an alumina tube, which was mounted horizontally inside a high temperature furnace. ZnO powders (99.9% purity, Fisher Chemicals) were placed on an alumina wafer, and loaded in the center of the tube. The tube was firstly heated up to 800 °C at a rate of 20 °C min^{-1} and kept for 30 min, followed by further heating up to a specific target temperature (details can be found in Table 1) at a constant rate of 15 °C min^{-1} and kept for 6 hours. During the experiment an Ar–5% H_2 gas mixture was introduced as the carrier gas. A specific total pressure (Table 1) was also maintained throughout the experiment. In the annealing experiment, the gas was swapped to pure O_2 with a flow rate of 100 sccm for 2 hours right after the deposition. Several series of experiments, including temperature series, pressure series and two O_2-annealing series, were systematically conducted in order to study the growth mechanism of the nanocable heterostructures. Detailed experimental parameters of different series can be found in Table 1. The general morphology and chemical composition of the products were examined by scanning electron microscopy (SEM, LEO

† Electronic supplementary information (ESI) available: SEM and XRD. See http://www.rsc.org/suppdata/jm/b4/b400646a/

DOI: 10.1039/b400646a

Table 1 Experimental conditions of different fabrication series

	Sample No.	Target Temperature/°C	Total Pressure/mbar	Annealing in O_2	Actual Annealing Temperature/°C
Temperature Series	A1	1000	300	No	—
	B1	1200	300	No	—
	C	1300	300	No	—
Pressure Series	A1	1000	300	No	—
	A3	1000	500	No	—
Annealing Series (I)	B1	1200	300	No	—
	B2	1200	300	Yes	~300
Annealing Series (II)	A1	1000	300	No	—
	A2	1000	300	Yes	~300

1450 VP) with an energy dispersive X-ray (EDX) spectrometer attached to the same microscope. Powder X-ray diffraction (XRD, Rigakau RU-300) with Cu $K\alpha_1$ radiation was employed to examine the crystallinity of the products. Transmission electron microscopy (TEM, Philips CM120 and Tecnai 20 FEG) was used to investigate the microstructures of the products. Cathodoluminescence (CL) spectra were taken in a scanning electron microscope (SEM, Cambridge S360) using a MonoCL system (Oxford Instrument).

III. Results

General

The final products were obtained in the downstream of the alumina tube. The typical morphology of the products is demonstrated in the SEM image which can be found in the electronic supplementary information.† The products entangled with each other and curved wire-like morphologies with wire length up to several tens of micrometers are observed. The diameters of the products are fairly uniform at ~100 nm. A powder X-ray diffraction of the typical product can also be found in the electronic supplementary information.† All of the diffraction peaks can be indexed to hexagonal Zn (a = 2.665 Å, c = 4.947 Å) and ZnO (a = 3.25 Å, c = 5.207 Å), respectively. Similar results are obtained from all of the products synthesized under different experimental conditions. The XRD results suggest that the products are composed of crystalline Zn and ZnO.

Detailed microstructures of these "nanowires" are disclosed by TEM investigations. Fig. 1a is a typical low-magnification TEM image of the nanowires. The light/dark/light contrast observed along the nanowire radial direction suggests a different phase composition, indicating the core–shell cable structure. The selected area diffraction pattern (SADP) of the nanocables, as shown in Fig. 1b, reveals two sets of diffraction spots, which correspond to those from the Zn <110> zone and the ZnO <110> zone, respectively. Fig. 1c and d are the dark field TEM images using Zn ($1\bar{1}0$) and ZnO ($1\bar{1}0$) diffraction spots, respectively. It shows that the Zn and the ZnO are locates in the nanocable's core and shell regions, respectively.

Temperature series

Samples A1, B1 and C were fabricated under the same experimental conditions except the target temperature, which was kept at 1000, 1200 and 1300 °C, respectively (Table 1). The low-magnification TEM image of a typical wire in sample A1 is shown in Fig. 2a, revealing the Zn-core/ZnO-shell cable structure. Fig. 2c is a high-resolution TEM (HRTEM) image of the same sample, disclosing a smooth surface of the ZnO layer and a sharp interface between Zn and ZnO. An epitaxial relationship between Zn and ZnO was suggested by both the SADP and the high-resolution image (Fig. 2b and c, respectively). Nevertheless, such epitaxy is not perfect, as the ZnO diffraction spots are slightly elongated, suggesting a small distribution of the ZnO orientation with respect to that of the Zn core (single crystalline). This is also observed in the high-resolution image.

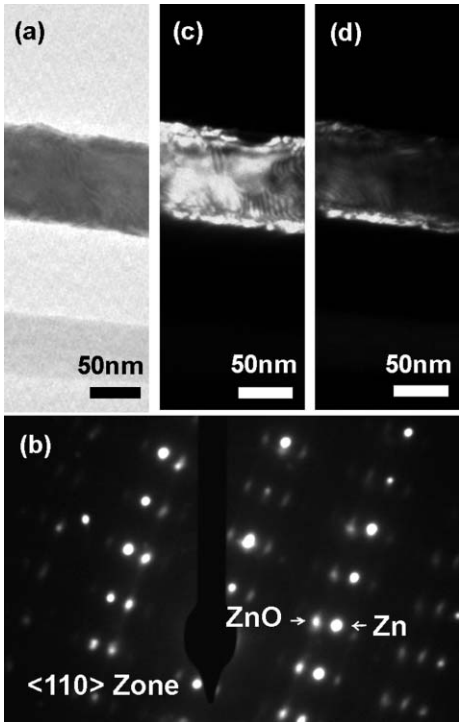

Fig. 1 (a) Low-magnification bright-field TEM image of the nanocable; (b) SADP of the nanocable; (c) dark-field TEM image of the nanocable taken by choosing Zn ($1\bar{1}0$) diffraction spot; (d) dark-field TEM image of the nanocable taken by choosing ZnO ($1\bar{1}0$) diffraction spot.

Fig. 2d shows the low magnification TEM image of a typical wire in sample B1, a similar core–shell cable structure as that of sample A1 is observed. The SADP and HRTEM image (Fig. 2e and f, respectively) confirm that the Zn/ZnO interface has a good epitaxial relationship and both Zn and ZnO maintain a good single crystallinity. Nevertheless, both the Zn/ZnO interface and the oxide surface are rough.

The TEM images of a typical wire in sample C are shown in Fig. 2g–i. Good epitaxial relation of Zn/ZnO is reflected from both the SADP and the HRTEM image as shown in Fig. 2h and i, respectively. However, the roughness of both the interface and the oxide layer surface increases compared to those of sample B1. The thicknesses of the oxide layer of the nanocables in sample A1, B1 and C are similar, *i.e.*, in the range of a few nanometers.

The room temperature CL spectra of samples A1, B1 and C are shown in Fig. 6a (later). Two emission peaks are observed

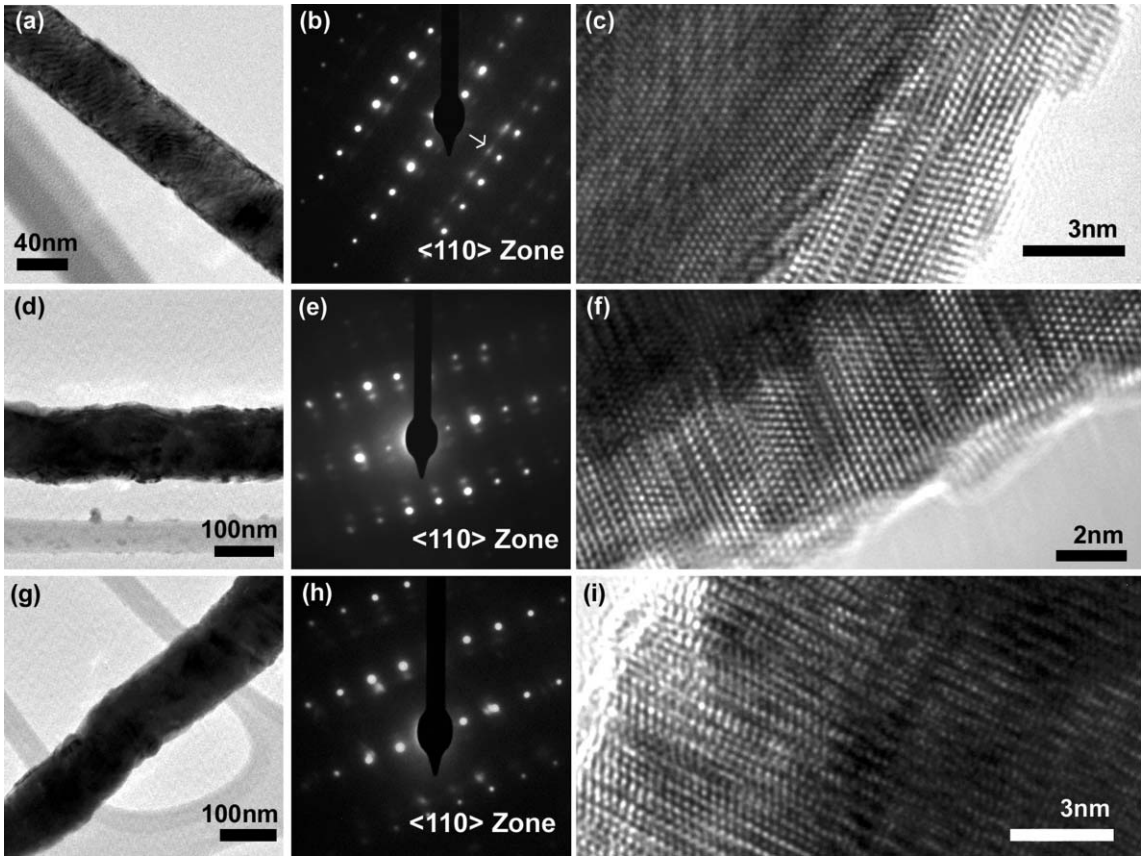

Fig. 2 (a) Low-magnification TEM image of a typical wire in sample A1; (b) SADP of sample A1 from $<110>$ zone. The elongated ZnO spots are marked by arrows; (c) HRTEM of sample A1. A sharp Zn/ZnO interface is clearly observed; (d) low-magnification TEM image of a typical wire in sample B1; (e) SADP of sample B1, which reveals the epitaxial relationship between the Zn core and the ZnO outer shell; (f) HRTEM of sample B1, confirming the crystallinity and the epitaxial relationship; (g) low-magnification TEM image of a typical wire in sample C; (h) SADP of sample C; (i) HRTEM of sample C, showing a rough Zn/ZnO interface and oxide surface.

in the spectra, where the UV emission at $\sim$390 nm is identified as the band edge emission of ZnO,[30] and the green emission peaked around 535 nm relates to the point defects in the ZnO layer.[31–33] The band edge to the defect emission (B/D) ratio of sample A1 is the highest while that of sample C is the lowest.

Pressure series

In this series, samples A1 and A3, which were deposited under different total pressure, are compared.

Fig. 3 shows the TEM images of a typical wire from sample A3. The HRTEM image (Fig. 3b) shows the oxide layer is also a few nanometers thick, which is similar to that of Al. Together with the diffraction pattern (Fig. 3c), the high-resolution image suggests that some epitaxial relationship exists between the Zn and the ZnO. Compared to sample A1, the interface and the oxide layer surface of sample A3 become rough, and part of the ZnO layer becomes polycrystalline. The CL spectra of samples A1 and A3 in Fig. 6b reveal a higher B/D ratio in sample A1 than in A3.

Annealing series

Samples B1 and B2 were both fabricated at 1200 °C, while B2 had an additional 2 hours *in-situ* annealing in the O_2 environment. The TEM images of a typical wire in sample B2 are shown in Fig. 4. Compared to those of sample B1, the nanocable structure and the epitaxial relationship between Zn and ZnO remain good, the oxide layer thickness increases slightly after annealing. The CL spectra of samples B1 and B2

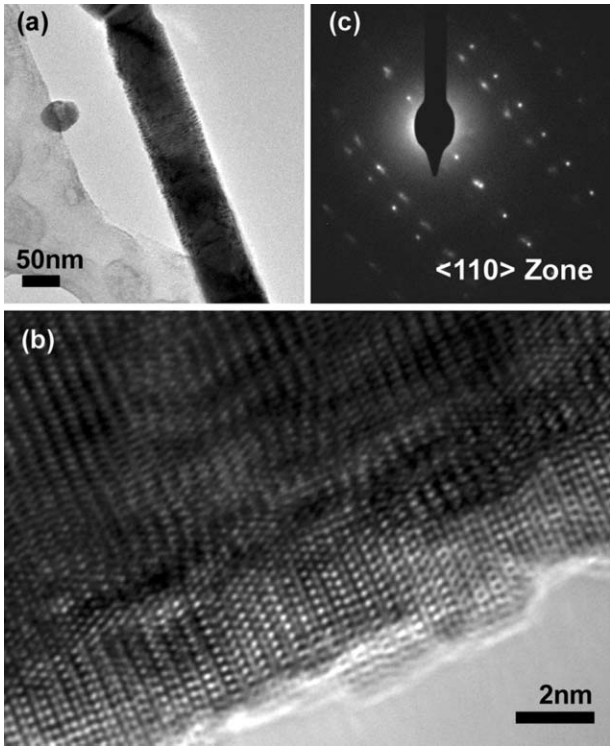

Fig. 3 (a) TEM image of a typical wire in sample A3; (b) HRTEM of the same sample; (c) SADP of the same sample, diffraction spots corresponding to ZnO are elongated.

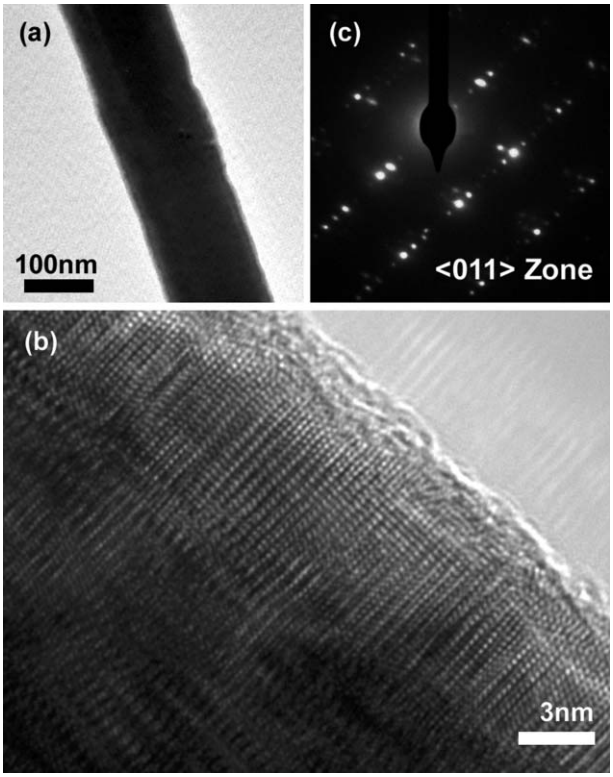

Fig. 4 (a) TEM image of a typical wire in sample B2; (b) HRTEM image of the same sample. An epitaxial relationship can be found between the Zn core and the ZnO outer shell; (c) SADP of the sample.

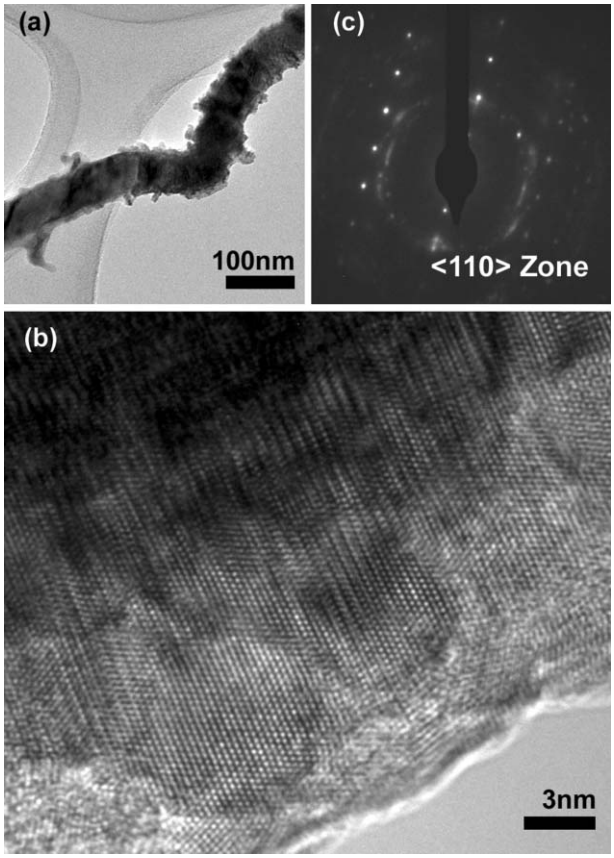

Fig. 5 (a) TEM image of a typical wire in sample A2; (b) HRTEM image of the same sample, where the ZnO layer becomes polycrystalline; (c) SADP of the sample. While the Zn core remains single crystalline, the diffraction spots of ZnO become a ring-like pattern, revealing the polycrystalline nature of the ZnO.

in Fig. 6c show that the B/D ratio of sample B2 is higher than that of B1.

Samples A1 and A2 form another annealing series that we had studied. Both of them are fabricated at 1000 °C and sample A2 has an additional 2 hours *in-situ* annealing in O_2. The results for sample A1 were described above. The oxide layer of the wire in sample A2 also becomes thicker after annealing. Compared to those of sample A1, the TEM images of A2 (in Fig. 5) show that the interface is not sharp and the oxide layer surface becomes rough after annealing. The SADP in Fig. 5c further suggests that the epitaxial relationship between Zn and ZnO is much worsened and the ZnO becomes polycrystalline with grain size ~2.5 nm. An epitaxial relationship is only found in limited regions (as shown in Fig. 5b). From the CL spectra of samples A1 and A2 (Fig. 6d), we found that the B/D ratio of A1 is higher than that of A2.

IV. Discussion

In general, all the products have coaxial cable configurations with ZnO as the outer shells wrapping the Zn cores. Both X-ray diffraction and TEM studies show that both Zn and ZnO are crystalline. Nevertheless, while the Zn core is single crystalline in all of the samples, the crystallinity of the oxide layer depends on the fabrication conditions.

The 1D Zn/ZnO nanocable growth was based on the thermal reduction of ZnO by H_2:

$$ZnO + H_2 = Zn + H_2O$$

The reduced Zn vapor will be brought to the downstream of the alumina tube by the processing gas Ar. The Zn vapor will condense at the downstream of the tube, where the temperature is low due to the temperature gradient of the tube furnace. The controlled low supersaturation results in preferential one-dimensional growth.[34,35] While the nucleation and growth of Zn itself does not automatically introduce a surface oxide layer, the oxygen gas residual is always available owing to the low-vacuum limitation of the system (base pressure $\sim 10^{-2}$ Torr). The surface of the Zn nanowire is easily oxidized to ZnO in such an environment. This ZnO limits the lateral growth of the Zn "nanowire", resulting in the Zn core–ZnO shell nanocable morphology. Further oxidation requires O_2 diffusion through the already formed ZnO layer, which limits the rate of further oxidation, and thus the thickness of the ZnO layer.

Temperature series

The results of samples A1, B1 and C show that the increase in target temperature leads to an increase in the interface and the oxide surface roughness. Higher fabrication temperature leads to a higher supersaturation of the Zn vapor, which results in a non-uniform growth of the Zn core, and thus the surface oxide layer.

The ZnO layer is formed by oxidizing the Zn surface, and epitaxy is made possible due to the geometrical similarity between the hexagonal Zn and ZnO. In the ZnO formation process, higher temperature contributes to the better epitaxial relationship as it increases the mobility of the depositing atoms.[36] This is consistent with our experimental observations of samples deposited from 1000–1300 °C. where better epitaxy is observed as temperature increases.

Two emission peaks are observed in the CL spectra as shown in Fig. 6a. The band edge emission at ~390 nm is normally observed at room temperature in large ZnO crystals with good crystallinity and high purity, indicating the good quality of its electronic structure.[30,37,38] The deep level emission (~535 nm) is mainly ascribed to the oxygen vacancies present in the ZnO layer.[31–33] Such oxygen vacancies are common in II–VI materials such as ZnO, especially when the ZnO results from oxidation of Zn and the O concentration in the gas phase is low (similar to our experimental conditions). Fig. 6a shows a

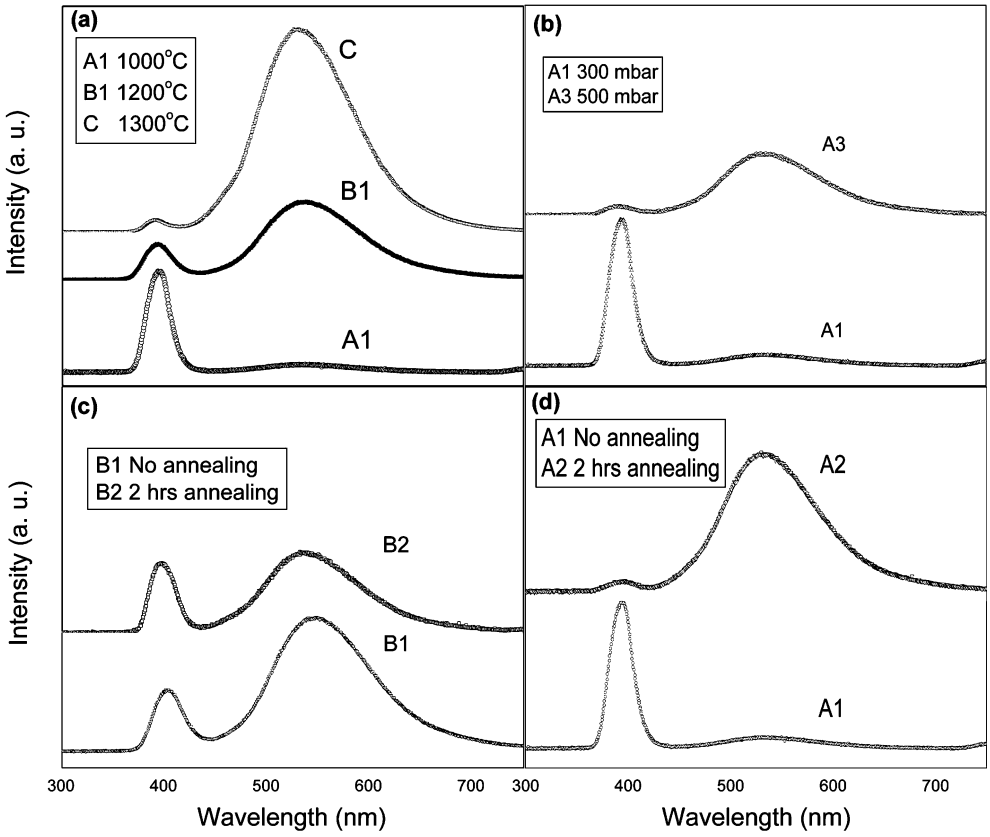

Fig. 6 (a) CL spectra taken at room temperature from samples A1, B1 and C; (b) CL spectra of samples A1 and A3 taken at room temperature; (c) CL spectra of samples B1 and B2 taken at room temperature; (d) CL spectra of samples A1 and A2 taken at room temperature.

decreased B/D ratio when the target temperature increases, indicating the increased O vacancies in the ZnO, which is also consistent with the ZnO formation mechanism, *i.e.*, elevated temperature is more likely to result in an O deficiency in ZnO during the Zn oxidation process.[39]

Pressure series

Higher fabrication pressure also leads to a rougher interface and oxide surface, due to a similar effect as that of the temperature, *i.e.*, a higher supersaturation of the Zn vapor results in the non-uniform Zn growth and thus the rough oxide surface.

The CL emission due to O vacancies is lower in the product that was fabricated at lower pressure (Fig. 6b). Assuming similar gas leakage and pumping speed of the system at both total pressures, lower total pressure is associated with a higher O_2 partial pressure, which contributes to the lower level of oxygen vacancies in the crystal.

Annealing series at 1200 °C

From the TEM images of samples B1 and B2, we observed that the thickness of the oxide layer only slightly increased after annealing in the O_2 environment. The slightly increased ZnO layer thickness may be ascribed to the relatively low bulk diffusion rate of O_2 at low temperature ($\sim$300 °C) in ZnO with good crystallinity (the situation in sample B1, in which single crystallinity of both Zn and ZnO is demonstrated).[40–42] The newly formed ZnO in the annealing process follows the structure of the oxide layer that already existed, and the epitaxial relation is largely maintained after annealing.

The CL spectra (Fig. 6c) show that the B/D ratio becomes higher after annealing. As the O_2 contributes very little to the further ZnO growth in the limited annealing period (2 h), it mainly anneals the O_2 vacancies in the existing ZnO lattice due to the slow diffusion process.

Annealing series at 1000 °C

Comparing the oxide layers of samples A1 and A2, the oxide surface of sample A2 becomes very rough and the oxide becomes polycrystalline. These are quite different from those observed in the 1200 °C annealing series. The ZnO layer in sample A1 is no longer single crystalline (as seen from the SADP in Fig. 2b). The presence of grain boundaries facilitates the oxygen diffusion process (grain boundary diffusion *vs.* bulk diffusion), leading to non-uniform oxidation along the whole length of the nanowire, and finally a polycrystalline ZnO layer and a rough oxide layer surface.

Consequently, the amount of oxygen vacancies in the ZnO increases (as seen from the CL spectra in Fig. 6d), as oxygen mainly contributes to further oxidation of Zn instead of annealing the existing oxygen vacancies in the ZnO crystallites. In addition, increased numbers of grains are created during the annealing process, which results in an increased surface to volume ratio of the oxide layer. This may further contribute to the O defect density.[43,44]

V. Conclusions

In conclusion, uniform coaxial Zn/ZnO nanocables were synthesized *via* thermal reduction of ZnO using H_2. Both the Zn core and the ZnO outer shell are crystalline, and CL spectra of the samples reveal peaks in both the UV and the visible regime, corresponding to the emissions from ZnO. A better Zn/ZnO epitaxy and ZnO crystallinity can be achieved by increasing the fabrication temperature. Nevertheless, the same factor leads to higher O deficiency in the ZnO layer. Increasing the fabrication pressure with the current experimental setting results in degradation of the ZnO crystallinity as well as more O defects in the oxide layer. The quality of the ZnO layer in the as-deposited nanocable determines the crystallinity of the ZnO after annealing, *i.e.* further oxidation of the Zn core *via* lattice

diffusion of the single crystalline ZnO shell results in reduced O defect density and preserved Zn/ZnO epitaxy; while further oxidation through ZnO grain boundaries deteriorates the epitaxy. In general, the thickness of the ZnO layer can be controlled by the post-annealing duration, *e.g.* the ZnO thickness for samples with Zn/ZnO epitaxy can be increased from $\simeq$5 nm (as-synthesized) to $\simeq$20 nm after 6 h annealing, and would be even larger ($\simeq$30–40 nm) for samples without the Zn/ZnO epitaxy. This provides us with a solution to synthesize Zn/ZnO nanocables with desired oxide layer thickness and ZnO crystallinity, which may have applications in various optoelectronic nanodevices.

Acknowledgements

This research is supported by the RGC direct allocation in the Chinese University of Hong Kong under project No. 2060227.

References

1 J. Goldberger, R. He, Y. Zhang, S. Lee, H. Yan, H.-J. Choi and P. Yang, *Nature*, 2003, **422**, 599.
2 C. L. Cheung, A. Kurtz, H. Park and C. M. Lieber, *J. Phys. Chem. B*, 2002, **106**, 2429.
3 C. C. Tang, S. S. Fan, H. Y. Dang, P. Li and Y. M. Liu, *Appl. Phys. Lett.*, 2000, **77**, 1961.
4 Y. Yin, G. Zhang and Y. Xia, *Adv. Funct. Mater.*, 2002, **12**, 293.
5 L. J. Lauhon, M. S. Gudiksen, D. Wang and C. M. Lieber, *Nature*, 2002, **420**, 57.
6 Y. Wu and P. Yang, *Appl. Phys. Lett.*, 2000, **77**, 43.
7 Y. Xie, P. Yan, J. Lu, Y. Qian and S. Zhang, *Chem. Commun.*, 1999, 1969.
8 A. M. Morales and C. M. Lieber, *Science*, 1998, **279**, 208.
9 Y. Zhang, K. Suenaga, C. Colliex and S. Iijima, *Science*, 1998, **281**, 973.
10 Y. Xie, Z. Qiao, M. Chen, X. Liu and Y. Qian, *Adv. Mater.*, 1999, **11**, 1512.
11 Q. Li and C. Wang, *J. Am. Chem. Soc.*, 2003, **125**, 9892.
12 X. Duan, Y. Hung, Y. Cui, J. Wang and C. M. Lieber, *Nature*, 2001, **409**, 66.
13 Y. Huang, X. Duan, Q. Wei and C. M. Lieber, *Science*, 2001, **291**, 630.
14 Y. Cui and C. M. Lieber, *Science*, 2001, **291**, 851.
15 H. Kind, H. Yan, B. Messer, M. Law and P. Yang, *Adv. Mater.*, 2002, **14**, 158.
16 X. Duan, Y. Huang, R. Agarwal and C. M. Lieber, *Nature*, 2003, **421**, 241.
17 H. Z. Zhang, D. P. Yu, Y. Ding, Z. G. Bai, Q. L. Hang and S. Q. Feng, *Appl. Phys. Lett.*, 1998, **73**, 3396.
18 Y. F. Zhang, Y. H. Tang, H. Y. Peng, N. Wang, C. S. Lee, I. Bello and S. T. Lee, *Appl. Phys. Lett.*, 1999, **75**, 1842.
19 Y. Cui, L. J. Lauhon, M. S. Gudiksen, J. Wang and C. M. Lieber, *Appl. Phys. Lett.*, 2001, **78**, 2214.
20 C. Li, D. Zhang, S. Han, X. Liu, T. Tang and C. Zhou, *Adv. Mater.*, 2003, **15**, 143.
21 H. Y. Peng, Z. W. Pan, L. Xu, X. H. Fan, N. Wang, C.-S. Lee and S.-T. Lee, *Adv. Mater.*, 2001, **13**, 317.
22 C. Ma, D. Moore, J. Li and Z. L. Wang, *Adv. Mater.*, 2003, **15**, 228.
23 H. Yan, R. He, J. Pham and P. Yang, *Adv. Mater.*, 2003, **15**, 402.
24 Y. Jiang, X.-M. Meng, J. Liu, Z.-Y. Xie, C.-S. Lee and S.-T. Lee, *Adv. Mater.*, 2003, **15**, 323.
25 Y.-C. Zhu and Y. Bando, *Chem. Phys. Lett.*, 2003, **372**, 640.
26 C. Pacholski, A. Kornowski and H. Weller, *Angew. Chem., Int. Ed.*, 2002, **41**, 1188.
27 J.-J. Wu, S.-C. Liu, C.-T. Wu, K.-H. Chen and L.-C. Chen, *Appl. Phys. Lett.*, 2002, **81**, 1312.
28 J. Q. Hu, Q. Li, X. M. Meng, C. S. Lee and S. T. Lee, *Chem. Mater.*, 2002, **15**, 305.
29 Y. J. Xing, Z. H. Xi, Z. Q. Xue, X. D. Zhang, J. H. Song, R. M. Wang, J. Xu, Y. Song, S. L. Zhang and D. P. Yu, *Appl. Phys. Lett.*, 2003, **83**, 1689.
30 V. Srikant and D. R. Clarke, *J. Appl. Phys.*, 1998, **83**, 5447.
31 K. Vanheusden, C. H. Seager, W. L. Warren, D. R. Tallant and J. A. Voigt, *Appl. Phys. Lett.*, 1996, **68**, 403.
32 K. Vanheusden, W. L. Warren, C. H. Seager, D. R. Tallant, J. A. Voigt and B. E. Gnade, *J. Appl. Phys.*, 1996, **79**, 7983.
33 X. L. Wu, G. G. Siu, C. L. Fu and H. C. Ong, *Appl. Phys. Lett.*, 2001, **78**, 2285.
34 W. B. Campbell, in *Whisker Technology*, ed. A. P. Levitt, Wiley-Interscience, New York, 1970, p. 15.
35 Y. Xia, P. Yang, Y. Sun, Y. Wu, B. Mayers, B. Gates, Y. Yin, F. Kim and H. Yan, *Adv. Mater.*, 2003, **15**, 353.
36 Y. J. Kim, Y. T. Kim, H. K. Yang, J. C. Park, J. I. Han, Y. E. Lee and H. J. Kim, *J. Vac. Sci. Technol., A*, 1997, **15**, 1103.
37 P. S. Xu, Y. M. Sun, C. S. Shi, F. Q. Xu and H. B. Pan, *Nucl. Instrum. Methods Phys. Res. B*, 2003, **199**, 286.
38 D. W. Hamby, D. A. Lucca, M. J. Klopfstein and G. Cantwell, *J. Appl. Phys.*, 2003, **93**, 3214.
39 O. Kubaschewski and B. E. Hopkins, in *Oxidation of Metals and Alloys*, Butterworths, London, 1962, p. 24.
40 W. N. Unertl and J. M. Blakely, *Surf. Sci.*, 1977, **69**, 23.
41 A. Krozer and B. Kasemo, *Surf. Sci.*, 1980, **97**, L339.
42 G. W. Tomlins and J. L. Routbort, *J. Am. Ceram. Soc.*, 1998, **81**, 869.
43 Y. W. Wang, L. D. Zhang, G. Z. Wang, X. S. Peng, Z. Q. Chu and C. H. Liang, *J. Cryst. Growth*, 2002, **234**, 171.
44 P. Yang, H. Yan, S. Mao, R. Russo, J. Johnson, R. Saykally, N. Morris, J. Pham, R. He and H.-J. Choi, *Adv. Funct. Mater.*, 2002, **12**, 323.